Surface zooplankton size and taxonomic composition in Bowdoin Fjord, north-western Greenland: A comparison of ZooScan, OPC and microscopic analyses

Akihiro Naito[a,1], Yoshiyuki Abe[a,b], Kohei Matsuno[a,b], Bungo Nishizawa[a,b], Naoya Kanna[b,c], Shin Sugiyama[b,c], Atsushi Yamaguchi[a,b,d*]

[a] Graduate School of Fisheries Science, Hokkaido University, 3-1-1 Minato-cho, Hakodate, Hokkaido, 041-8611, Japan

[b] Arctic Research Centre, Hokkaido University, Kita-21 Nishi-11 Kita-ku, Sapporo, Hokkaido, 001-0021, Japan

[c] Institute of Low Temperature Science, Hokkaido University, Kita-19 Nishi-8 Kita-ku, Sapporo, Hokkaido, 060-0819, Japan

[d] Biology Department, Woods Hole Oceanographic Institution, 266 Woods Hole Rd., Woods Hole, MA 02543, USA

* Corresponding author

E-mail: a-yama@fish.hokudai.ac.jp, ayamaguchi@whoi.edu (A. Yamaguchi)

[1] Present address: Nosui Co. Ltd., Mita Nitto Daibiru, 4th Floor, 3-11-36 Mita, Minato-ku, Tokyo, 108-0073, Japan

Abstract

In Greenland, tidewater glaciers discharge turbid subglacial freshwater into fjords, forming plumes near the calving fronts. To evaluate the effects of this discharge on the zooplankton community in the fjords, we collected sea surface zooplankton samples in Bowdoin Fjord in north-western Greenland during the summer of 2016 and made microscopic, OPC and ZooScan analyses. Within the three quantitative methods, ZooScan has advantages that can evaluate various parameters (e.g., abundance, biomass, size and taxonomic information) simultaneously and has the ability to eliminate abiotic particles, such as silt and sediment, which are abundant in samples. Based on taxonomic biomass data, the zooplankton community is clustered into three groups, which varied spatially: inner, middle and outer fjord groups. Jellyfish dominated the outer fjord group, and barnacle cypris larvae dominated the middle fjord group. For the inner fjord group, large-sized *Calanus* spp. and chaetognaths were abundant. Since these species are characterized with oceanic taxa, they would intrude through the deep fjord water and subsequently be upwelled through entrainment of glacially modified plume water. From the NBSS analysis on zooplankton size spectra, the steep slope of NBSS in the middle fjord community suggests that the high productivity was caused by the addition of meroplanktonic cypris larvae.

Keywords

glacial fjord, Bowdoin Fjord, zooplankton, ZooScan, NBSS

1. Introduction

Recently, tidewater glaciers in Greenland have been thinning and retreating under the influence of atmospheric warming (e.g., Howat and Eddy, 2011; Murray et al., 2015). These glaciers flow directly into the ocean, forming an important ice-ocean boundary in a glacial fjord. Near the glacier front, subglacial discharge upwells and forms a sediment-rich turbid meltwater plume (Chu, 2014; Ohashi et al., 2016; Kanna et al., 2018). In front of tidewater glaciers, particularly near the plume, dense occurrences of marine mammals and sea birds are commonly observed (Hop et al., 2002; Lydersen et al., 2014; Dalpadado et al., 2016; Arimitsu et al., 2016). These aggregations of marine mammals and sea birds at meltwater plumes in glacial fjords suggest that their food, especially zooplankton, may be higher than in other regions. However, sampling and measurements are difficult near the glacier front; thus, little information on zooplankton abundance is available in glacial fjords near the plumes.

For the evaluation of zooplankton, size and taxa are two important proxies to evaluate their quantitative and qualitative roles. Using size spectra zooplankton biomass data, calculation of normalized biomass size spectra (NBSS) provides valuable information on zooplankton productivity, energy transfer efficiency and their prey-predator linkages (Zhou, 2006; Zhou et al., 2009). While important, size measuring zooplankton by microscopic observations is time consuming. Taxonomic identification under a microscope also requires knowledge of zooplankton taxa. To overcome these problems, several instruments have been developed. An Optical Plankton Recorder (OPC) using light attenuation is an instrument that can quantify zooplankton in 4096 size categories between 0.25 and 5.0 mm using the Equivalent Spherical Diameter (ESD) in a short time (Herman, 1988, 1992). While useful, the OPC does not provide taxonomic

63 information. An instrument that measures both size and taxonomic information at the
64 same time, the zooplankton scanning image analysis system (ZooScan) was established
65 (Gorsky et al., 2010). ZooScan has been used in various locations (e.g., Abrolhos Bank,
66 Bay of Biscay, off Ubatuba, Brazil and others) (Marcolin et al., 2013, 2015; Vandromme
67 et al., 2014). However, little information is available for inter-calibration with other
68 instruments, which prevents the evaluation of measurement characteristics of the
69 ZooScan.

70 In the present study, we studied the size and taxonomic composition of sea-
71 surface zooplankton in Bowdoin Fjord, a glacial fjord located in north-western Greenland
72 during July 2016. Zooplankton samples, collected by sea-surface tow at fifteen stations
73 set from the plume to the outside along with fjord, were preserved. Using the same
74 zooplankton samples, their size spectra were quantified by OPC and ZooScan, and
75 taxonomic accounts were also identified with ZooScan and microscopic observations.
76 Applying size-mass relationships, zooplankton biomass (wet mass: WM) derived by OPC
77 and ZooScan were compared with directly measured WM. Finally, the calculation of
78 NBSS based on OPC and ZooScan may enable us to evaluate the measurement
79 characteristics (causes of under/over estimation) of each instrument and the regional
80 characteristics of zooplankton in the glacial fjord.

81 **2. Materials and methods**

82 *2.1. Field sampling*

83 Bowdoin Glacier (77°41'N, 68°35'W) is a marine-terminating glacier located along the
84 coast of Prudhoe Land in north-western Greenland (Sakakibara and Sugiyama, 2018).
85 The glacier flows into Bowdoin Fjord at a rate of ~500 m $year^{-1}$ and discharges icebergs

and meltwater through a 3-km wide calving front (Fig. 1a) (Sugiyama et al., 2015). The glacier is ~280 m thick and the fjord is ~250 m deep near the calving front. Boat-based observations were made in the daytime during 27-29 July 2016. Temperature and salinity at 2 m were measured with a CTD profiler (ASTD 102, JFE Advantech, Japan) at 44 stations, which encompassed the plume through to the outside of the fjord (data from Kanna et al., 2018). At 15 stations, a horizontal tow of a single-NORPAC net (mouth diameter 45 cm, mesh size 335 μm) at 2-3 m was made over three minutes. To register the filtered water volume, a flowmeter (Rigosha, Saitama, Japan) was mounted in the mouth of the net. The net sampling depth was also monitored by a depth recorder (DEFI2-D50, JFE Advantech, Japan). Zooplankton samples were preserved with borax-buffered formalin by adding 5% volume to the total zooplankton samples.

2.2 Microscopic observation and wet mass measurement

In the laboratory, microscopic observations were made of subsamples (1/4 to 1/32) made by a Motoda splitter (Motoda, 1959) according to the size of samples. Species and taxonomic identifications, sorting and counting were made under a stereomicroscope (Nikon SMZ800N). Taxa except copepods were counted with taxon (e.g. jellyfishes, chaetognaths, appendicularians, euphausiids, polychaetes, barnacles). For copepods, classification of *Calanus* spp. and other species was made. The sorted samples were placed on pre-weighed mesh (100 μm), seawater was removed with aid of tissue, then the wet mass (WM) was measured with a microbalance (Mettler Toledo AE100) with the precision of 0.1 mg. All abundance and biomass data are shown as per cubic metre (ind. m^{-3} or mg WM m^{-3}).

2.3 OPC measurement

OPC measurements were made with a bench-top OPC (Model OPC-1L: Focal Technologies Corp.) using 1/2-1/128 subsamples (varied according to the size of the samples) of the total formalin-preserved samples. OPC measurements were made at a low flow rate (ca. 10 L min^{-1}) and low particle density (<10 counts s^{-1}) without staining (Yokoi et al., 2008).

The abundance per cubic metre (*N*: ind. m^{-3}) for each of the 4,096 ESD size categories was calculated using the following equation:

$$N = \frac{n}{s \times F}$$

where *n* is the number of particles (=zooplankton ind.), *s* is the split factor of each sample, and *F* is the filtered volume of the net (m^3). The biovolume of the zooplankton community in 4,096 size categories was calculated from the ESD data, and the biovolume (mm^3 m^{-3}) was calculated by multiplying *N* and the volume (mm^3 $ind.^{-1}$) derived from ESD. Zooplankton wet mass (WM) for 4,096 size categories was calculated from the ESD data by assuming the relative density of zooplankton to be equal to that of seawater (1 mg mm^{-3}). Analyses of the mesozooplankton biomass were performed with the separation of five size classes (0.335-1 mm, 1-2 mm, 2-3 mm, 3-4 mm, 4-5 mm ESD).

2.4 ZooScan measurement

Zooplankton images were scanned with a water-proof ZooScan (ZooScan MIII, Hydroptic Inc., France) using 1/4-1/128 subsamples (varied according to the size of the samples) of the total formalin-preserved samples. The overall process and analysis followed Gorsky et al. (2010). Before each measurement, background measurements were made by filling with deionized water. ZooScan measurements were made under

131 the condition that all zooplankton sank to the bottom of a scanning cell of 15 cm × 24 cm
132 in area. Zooplankton overlapping was avoided by using soft tweezers manually.
133 The obtained zooplankton images were separated from individual objects by the
134 ZooProcess software. Zooplankton images were digitalized at 2400 dpi resolution.
135 From this resolution, one pixel corresponded to 10.58 μm. For identification, all
136 obtained images were uploaded to the website EcoTaxa (http://ecotaxa.obs-vlfr.fr/prj/).
137 Images, identified as “detritus”, “fibre”, “artefact” and “other”, were removed for further
138 analyses. ZooScan provides estimates of body length (major axis of the best fitting
139 ellipse) and width (minor axis) (Gorsky et al., 2010). From these major and minor axes,
140 the biovolume was calculated: biovolume = $4/3\times\pi\times(\text{major axis})/2\times(\text{minor axis}/2)^2$.
141 From these biovolume data, the equivalent spherical diameter (ESD, μm) was computed
142 for each zooplankton object. Zooplankton wet mass (WM) was calculated from the ESD
143 data by assuming the relative density of zooplankton to be equal to that of seawater (1 mg
144 mm^{-3}).

145 *2.5 Data analysis*

146 To evaluate regional changes in the zooplankton community, a cluster analysis based on
147 biomass was performed. Zooplankton biomass data (*ZB*: mg WM m^{-3}) of each taxon
148 (jellyfishes, chaetognaths, appendicularians, euphausiids, polychaetes, barnacles,
149 *Calanus* spp. and other copepods) were normalized as $\log_{10}(ZB+1)$. Next, similarities
150 between zooplankton samples were calculated using the Bray-Curtis similarity index.
151 To group the samples, similarity indices were coupled with hierarchical agglomerative
152 clustering using a complete linkage method (Unweighted Pair Group Method using
153 Arithmetic mean: UPGMA; Field et al., 1982). These analyses were made with

PRIMER v7 (PRIMER-E Ltd.).

From OPC and ZooScan data, zooplankton biovolume ($mm^3\ m^{-3}$) between 0.335-5.0 mm ESD was summed at each 0.1-mm ESD size class interval. To calculate the *X*–axis of the NBSS (*X*: $\log_{10}$ zooplankton biovolume [mm^3 $ind.^{-1}$]), the biovolume was divided by the abundance of each size class (ind. m^{-3}) and converted to a common logarithm. To calculate the *Y*–axis of the NBSS (*Y*: $\log_{10}$ zooplankton biovolume [mm^3 m^{-3}]/Δbiovolume [mm^3]), the biovolume was divided by the interval of biovolume (Δbiovolume [mm^3]) and converted to a common logarithm. Based on these data, the NBSS linear model was calculated as follows:

$$Y = aX + b$$

where *a* and *b* are the slope and intercept of the NBSS, respectively.

To make comparisons of NBSS between OPC and ZooScan, a *U*-test was made. To evaluate whether the NBSS slope varied with the NBSS intercept or measured instruments, an analysis of covariance (ANCOVA) with the NBSS intercept and measured instruments (OPC or ZooScan) as independent variables was conducted. *U*-test analyses and an ANCOVA were performed using StatView v5 (SAS Institute Inc., Cary, NC, USA).

3. Results

3.1. Hydrography

Temperature at the 2-m depth ranged between 3.16-5.21°C, and decreased from the glacier to outer fjord, while it showed abrupt high temperatures at the farthest offshore station (Fig. 1b). Salinity was in the range of 13.62 to 30.52 and increased from the glacier plume to the outer fjord.

176 *3.2. Calibration*

177 Comparisons of abundance (ind. m^{-3}) and WM (mg WM m^{-3}) between OPC or ZooScan-
178 derived data and direct measurements were made (Fig. 2). Based on whole samples (n
179 =15), all measurements were highly correlated with each other (r^2=0.86-0.95, p<0.0001).
180 For abundance, both OPC and ZooScan underestimated more than microscopic
181 observations (by a factor of 0.71-0.78), while OPC:ZooScan had similar values (0.91)
182 (Fig. 2a). For biomass, while coefficients of determination were high (r^2=0.90-0.95),
183 differences due to measurement methods were greater than those for abundance. Thus,
184 within the same samples, ZooScan quantified the largest value, followed by direct
185 measurements, and OPC yielded the least value (Fig. 2b).

186 *3.3. Cluster analysis*

187 Based on directly measured zooplankton biomass, the zooplankton community was
188 separated into three groups (A, B and C) at 47.5% similarity (Fig. 3a). The horizontal
189 distribution of each group varied clearly (Fig. 3b). Thus, group A was mainly observed
190 in the outer fjord, while group B was concentrated at the centre of the plume in front of
191 the glacier. The other largest group C mainly occupied the middle of the fjord. For
192 each group, the dominant zooplankton taxa varied: jellyfishes dominated in group A,
193 chaetognaths and copepods dominated in group B, and barnacle larvae (cypris) dominated
194 in group C (Fig. 4).

195 *3.4. Inter-method comparison in taxa (ZooScan* vs *microscope)*

196 Within the three quantitative methods (OPC, ZooScan and microscope), taxonomic
197 information was obtained from the ZooScan and by the microscope. Subsequently,

198 combining directly measured WM with taxa, the taxonomic composition of zooplankton
199 abundance and biomass were compared between those from ZooScan and direct
200 quantification. The abundance showed little differences between direct measurement
201 and ZooScan (Fig. 4). On the other hand, biomass showed
202 overestimation/underestimation, which varied with taxa and station (Fig. 4).

203 Abundance showed significant correlations between ZooScan and microscopic
204 observations for all species/taxa, while biomass showed significant correlations for only
205 four taxa, which accounted for half of the eight taxa (Fig. 5). In detail, for abundance,
206 appendicularians, euphausiids and copepods (*Calanus* spp. and others) had nearly linear
207 (Y:X=0.97-1.03) correlations between the ZooScan and microscopic observations, while
208 jellyfishes, chaetognaths, polychaetes and barnacle larvae were underestimated by
209 ZooScan, with factors of 0.29-0.78 (Fig. 5). For biomass, while four taxa showed
210 significant correlations between ZooScan and direct measurements, their factors in
211 ZooScan were overestimations (1.26-2.94) for polychaete and barnacle larvae and
212 underestimations (0.22-0.33) for appendicularians and other copepods.

213 *3.5. Inter-method comparison in size (ZooScan vs. OPC)*

214 Zooplankton size properties in abundance and biomass were quantified by two methods:
215 OPC and ZooScan. For abundance, both methods showed the predominance of the
216 smallest size class (0.335-1 mm ESD) throughout the stations and had little differences
217 with quantitative methods (Fig. 6). On the other hand, for biomass, differences between
218 methods were detected. Thus, zooplankton group A was dominated by the small size
219 class in OPC, while it was dominated by the large size class in ZooScan. For
220 zooplankton group C, the opposite pattern was seen: i.e., dominance of the large size class

221 in OPC, while predominance of the small size class in ZooScan was observed (Fig. 6).

222 Comparison within size classes showed that the smallest size class (0.335-1 mm
223 ESD) was highly correlated between ZooScan and OPC both in abundance and biomass
224 (Fig. 7). For the other size classes, significant correlations were observed for the 2-3
225 mm size class in abundance and the 1-2 and 2-3 mm size classes in biomass. Common
226 patterns for these size classes were underestimations of ZooScan compared to OPC, with
227 factors of 0.21-0.28 (Fig. 7).

228 *3.6. Inter-method comparison in NBSS (ZooScan* vs *OPC)*

229 The results of the NBSS analysis based on OPC and ZooScan are shown in Table 1.
230 Slopes of NBSS based on OPC were -1.705 to -0.737 (mean±sd: -1.111±0.301) and those
231 by ZooScan were -1.516 to -0.229 (-0.778±0.394). Slopes of NBSS were more
232 moderate for ZooScan than those from OPC (*U*-test, $p<0.05$) (Fig. 8). Intercepts of
233 NBSS based on OPC were -1.306 to -0.245 (-0.736±0.352), and those by ZooScan were
234 -1.326 to -0.889 (-0.726±0.537). No significant differences were detected for intercepts
235 of NBSS between OPC and ZooScan (*U*-test, $p=0.958$). From NBSS plots, it was
236 notable that zooplankton biovolumes at smaller size classes were lower for ZooScan than
237 for OPC (Fig. 8). This was due to the elimination of abiotic particles (e.g., silt or sand)
238 from ZooScan data based on the imaging analysis. For NBSS slopes, an ANCOVA
239 analysis, applying NBSS intercepts and differences in instruments (OPC or ZooScan) as
240 the independent variables, detected significant differences only for the differences in the
241 instruments (Table 2).

242 **4. Discussion**

243 Through zooplankton sample analyses based on multiple methods (i.e., microscope, WM,
244 OPC and ZooScan measurements), various characteristics in the zooplankton community
245 in the glacial fjord were evaluated. In the following section, we discuss three
246 methodological notes in terms of taxonomic (ZooScan vs microscope), size and NBSS
247 (ZooScan vs OPC) first. Then, we discuss the factors governing zooplankton
248 community in the glacial fjord.

249 *4.1. Taxonomic comparison*

250 While important, taxonomic information of zooplankton was not quantified in optical
251 instruments such as OPC and LOPC (Herman, 1988; Nogueira et al., 2004). ZooScan
252 obtains images of zooplankton and quantifies both size and taxonomic data from images
253 (e.g., Vandromme et al., 2012). In this section, we compare taxonomic data from
254 ZooScan with microscopic counts (abundance) and direct WM measurements (biomass).
255 Zooplankton abundance based on ZooScan have pointed out the possibility of
256 underestimation of minor taxa/species due to the deviation or split of the samples (Colas
257 et al., 2018). As a quantification method for minor and large-sized species/taxa, gently
258 sieving through a 0.5-mm mesh and ZooScan measurements for each fraction have been
259 proposed (Grosjean et al., 2004). However, it requires twice the time and is difficult to
260 achieve for many samples (Colas et al., 2018). Underestimation of abundance due to
261 the use of subsamples is reported to be common for rare species/taxa (Gorsky et al., 2010).
262 This is considered to be the cause of the underestimation of abundance for two less
263 abundant taxa: jellyfishes and chaetognaths in this study (Fig. 5), while underestimations
264 for numerical dominant two taxa, polychaetes and barnacle larvae, would be caused by
265 the double-splitting effects (note that the splitting was available for both microscopic

266 counts and ZooScan measurements) or heterogeneous distribution of these taxa in the
267 samples.

268 For zooplankton abundance, a good correlation has been reported for automated
269 and manual analyses based on same images created by ZooScan (Gorsky et al., 2010),
270 while for zooplankton biomass, comparison between estimated values from ZooScan
271 measurements and directly measured mass have not been reported to date. For biomass
272 estimation using ZooScan, underestimation tends to occur for large-body sized organisms
273 and taxa through the use of subsamples, since they are rare (e.g., termed “subsample
274 effect”, cf. Colas et al., 2018). Fluctuations of ZooScan-derived biomass of
275 chaetognaths and euphausiids in this study would be caused by this subsample effect (Fig.
276 5). Interestingly, clear underestimation by ZooScan for appendicularian biomass
277 occurred in this study (Fig. 5). This may due to the shape of appendicularian tails, which
278 are often curved, affecting the automated measurements (Gorsky et al., 2010). The
279 transparency of appendicularians may also effect the underestimation of their biomass
280 (Herman, 1992). Concerning jellyfishes, the destruction of fragile organisms and
281 species-specific differences in colour (=differences in transparency) may affect size
282 measurements (Thompson et al., 2013). While a significant correlation pattern was not
283 detected in this study, zero or overestimation were the cases for jellyfishes (Fig. 5). This
284 may due to the underestimation by transparent body or overestimation of size due to the
285 extension of jellyfish bodies on the measurement frame of ZooScan. For polychaetes
286 and barnacles, the two overestimated taxa for ZooScan biomass, since most of them were
287 small sized meroplanktonic larvae, it is difficult to accurately measure the wet mass using
288 this method in this study. Thus, underestimation of directly measured wet mass would
289 be the case for these two taxa.

290 *4.2. Size comparison*

291 In this study, the size property of zooplankton was measured by OPC and ZooScan.
292 OPC measures the size of plankton by detecting the shade of planktonic particles created
293 by a light beam and quantified size with 4,096 size units (Herman, 1992). Since OPC
294 detects particle as shadows during flow through a channel, there are some potential
295 sources of underestimation and overestimation on counting or sizing. As the cause of
296 underestimation, underestimation in number by particle coincidence and underestimation
297 in size caused by zooplankton direction to the light beam or body transparency are argued
298 (Herman, 1992; Sprules et al., 1998; Zhang et al., 2000). Conversely, as the cause of
299 overestimation, overestimation in number by counting on non-zooplankton particles, such
300 as detritus and fragmentation of zooplankton body and overestimation in size by particle
301 coincidence, are reported (Sprules et al., 1998; Zhang et al., 2000). For ZooScan, since
302 ZooScan quantifies the biovolume of zooplankton by assuming a perfect spheroid shape,
303 their estimated biomass is reported to be constantly higher than those measured by OPC
304 (Schultes and Lopes, 2009). With such shortcomings, zooplankton biomass estimation
305 by ZooScan is preferred to those of OPC because of the elimination of the aforementioned
306 various under- and overestimations, which are inevitable for OPC measurements
307 (Schultes and Lopes, 2009).

308 In the present study, correlations between OPC and ZooScan were detected for
309 both abundance and biomass of the relatively small size classes (0.335-3 mm) (Fig. 7).
310 Within them, highly significant correlations (r^2=0.99, p<0.0001) were observed for the
311 smallest size fraction (0.335-1 mm). In detail, the abundance showed nearly an equal
312 factor between them (1.04), while the biomass of ZooScan was 1.44 times higher than

313 that of OPC. This discrepancy would be caused by the differences in the biovolume
314 measurement method in ZooScan (by assuming a perfect spheroid shape) mentioned
315 above (Schultes and Lopes, 2009), while in the 1-3 mm size classes, a considerable
316 underestimation by ZooScan (with a factor of 0.21-0.28 of OPC) occurred for both
317 abundance and biomass (Fig. 7). For OPC, overestimations of abundance and biomass
318 frequently occurred by including detritus count (overestimation in abundance) and size
319 measurements on overlapping particles through a light beam (overestimation in biomass)
320 (Sprules et al., 1998; Zhang et al., 2000). On the other hand, ZooScan can avoid the
321 overlapping of particles by manual manipulation before measurement and can remove
322 detrital material data through image analysis. In fact, we confirmed that detrital
323 materials were composed 88.2±12.7% of total particles (including both plankton and
324 detritus) in 1-3 mm size classes by ZooScan image analysis. Thus, removing data on
325 detrital materials may cause a greater underestimation of ZooScan than the data of OPC,
326 which includes whole particles (both plankton and detritus). These facts suggest that
327 ZooScan can provide more accurate data on plankton. Because of the lack of correlation
328 detected for large size classes (3-5 mm), since these large size classes contain few
329 individuals, variations due to sample split may induce the great variability in the
330 individuals who belong to these size classes.

331 *4.3. NBSS*

332 NBSS is a calculated linear expression based on zooplankton size and is treated as an
333 index of the status of marine ecosystems (Herman and Harvey, 2006; Marcolin et al.,
334 2015). The slope of NBSS represents zooplankton productivity, energy transfer
335 efficiency and their prey-predator linkages (Zhou, 2006; Zhou et al., 2009). The

intercept of NBSS is an index of standing stocks (Sprules and Munawar, 1986). The slope of NBSS at approximately -1 indicates a theoretical steady state (Sprules and Munawar, 1986). In general, slopes steeper than -1 indicate bottom-up control (Moore and Suthers, 2006), or high productivity with low transfer efficiency (Sprules and Munawar, 1986; Zhou, 2006). Slopes flatter than -1 indicate top-down control (Moore and Suthers, 2006), or low productivity with high transfer efficiency (Sprules and Munawar, 1986; Zhou, 2006).

Since the ZooScan analysis is based on images, abiotic materials such as silt and sand are able to be eliminated before analysis (Gorsky et al., 2010). On the other hand, OPC could not separate plankton and abiotic particles. From the NBSS slope comparison between ZooScan and *in situ* LOPC in the Bay of Biscay, Vandromme et al. (2014) reported that the NBSS slope by LOPC (mean±1 sd: -0.97±0.24) is steeper than those by ZooScan (-0.86±0.40), while in a similar comparison in the Abrolhos Bank, Marcolin et al. (2013) reported the opposite pattern: i.e., the NBSS slope of LOPC is slightly flatter than those of ZooScan. These differences would be caused by the differences in the dominant zooplankton taxa, community structure and treated size ranges. In the present study, we applied the same size ranges for the NBSS calculation of both ZooScan and OPC and eliminated abiotic particle data for the NBSS calculation of ZooScan. This approach provides high biomass values for OPC, especially at small sizes, and steeper slopes for OPC (-1.11±0.30) than those of ZooScan (-0.78±0.39) (Fig. 8).

For the intercept of NBSS, because of the overestimation in fragmentation of jellyfishes during course of quantification, *in situ* LOPC tends to overestimate more than those of ZooScan (Vandromme et al., 2014). In this study, the intercept of NBSS showed

no significant differences between those from OPC (mean±1 sd: -0.74±0.35) and ZooScan (-0.73±0.54) (*U*-test, $p = 0.958$). This finding may be observed because the abiotic particles eliminated from ZooScan analysis were mostly at smaller sizes, and their elimination had little effect on the NBSS intercept. Commonly, the NBSS intercept is correlated with the NBSS slope (cf. Matsuno et al., 2012). However, in this study, the NBSS slope has no correlation with the intercept, but has a correlation with the instrument (e.g., OPC or ZooScan) (Table 2). These facts suggest that the effect of elimination of abiotic particles in the ZooScan analysis may have a greater effect on the results of the NBSS slope. Thus, to make an accurate evaluation of the NBSS slope, NBSS calculations based on ZooScan, including elimination of abiotic particles, are recommended.

4.4. Zooplankton community in the fjord

For zooplankton community, it should be noted that our data is only a surface sampling. Data interpretation by the differences of the sampling method from the previous studies should be considered. In glacial fjords, the zooplankton community is known to be strongly affected by the advection of outer oceanic water (Aksnes et al., 1989). For instance, the composition of the oceanic copepod *Calanus* spp. is increased through the outer fjord and accounted for 90% of their biomass (Arendt et al., 2010). In the present study, zooplankton biomass in the outer fjord (group A) was dominated by jellyfishes, and the composition of *Calanus* spp. was low (0.56-9.59%) (Figs. 3, 4). For this reason, the sampling methods of this study (horizontal net tow at sea surface [2-3 m]) may also be considered. Concerning jellyfishes, the dominance of the jellyfishes for the water masses outside the fjord are reported (Palma et al., 2014). Bearing this in mind, the

383 dominance of jellyfishes outside the fjord yield their dominance for zooplankton
384 community group A.

385 For the zooplankton community in the middle of the fjord in Greenland, various
386 copepods were dominant: *Metridia longa, Pseudocalanus* spp., *Microsetella* spp. and
387 *Oncaea* spp. have been reported (Arendt et al., 2010; Swalethorp et al., 2015). However,
388 in the present study, the zooplankton biomass of group C, observed in the middle of the
389 fjord, was dominated by barnacle cypris larvae (Figs. 3, 4). Concerning cypris larvae in
390 the fjord environment, Swalethorop et al. (2015) reported that cypris larvae were
391 abundant in the outer fjords in Greenland. These discrepancies may be related to
392 differences in sampling period (June or July), latitude (77.5ºN vs 64-65ºN) and currents
393 in each fjord. In the present study, the slope of the NBSS of group C (-0.915±0.368)
394 was steeper than those of the other groups (-0.745±0.434) (Fig. 8 and Table 1). It
395 suggests that high productivity occurred in the middle of the fjord. The steeper NBSS
396 slope of group C would be caused by the dominance of small-sized cypris larvae. Since
397 meroplanktonic larval phase of barnacles is limited for 2-3 weeks (Herz, 1933), these
398 steeper NBSS slopes of group C in the middle of the fjord would be moderate, and the
399 productivity would decrease after one month of this study.

400 For the inner fjords near glaciers in Greenland, the dominance of the copepods
401 *M. longa* and *Pseudocalanus* spp. has been reported (Swalethorp et al., 2015). This may
402 due to high biomass of their prey: i.e., protozooplankton, rotifer and copepod nauplii are
403 available there, and it implies favourable food conditions for copepods (Calbet et al.,
404 2011; Riisgaard et al., 2014; Swalethorp et al., 2015). Since there is a high gradient of
405 suspended particulate matter in inner fjords, species-specific differences in tolerance for
406 high sediment loads may explain their distribution (Arendt et al., 2011). For the glacial

fjord, subglacial discharge upwells and forms a sediment rich turbid meltwater plume (Chu, 2014). In the plume, high concentrations of suspended materials may affect feeding, egestion and reproduction of copepods. The ability to tolerate sediment is likely high for *M. longa* and low for *Calanus* spp., which determine their horizontal distribution:, i.e., *M. longa* and *Calanus* spp. occurred in the inner fjords and outer ocean, respectively (Arendt et al., 2011).

In glacial fjords, the input of glacial meltwater provides nutrients and induces high primary production in the inner parts of the fjord (Arendt et al., 2010). In our study region of Bowdoin Fjord, tidewater glaciers discharge turbid subglacial freshwater into fjords, forming a plume and providing macronutrient by upwelling near the calving front (Kanna et al., 2018). Through enhanced primary production, high productivity of zooplankton is expected in front of the glacier. However, the slope of NBSS for zooplankton group B, which was observed near the glacier, did not vary with the other groups (p=0.769, one-way ANOVA). This indicates moderate zooplankton productivity there. Concerning taxonomic composition, the zooplankton community of group B contained a high composition of *Calanus* spp. and chaetognaths, instead of the reported species/taxa (e.g., *M. longa* and *Pseudocalanus* spp.). Since both *Calanus* spp. and chaetognaths are characterized with oceanic species (Arendt et al., 2010), the occurrence of them near the calving front in this study suggests that there was inflow from oceanic water through the bottom of the fjord and upwelling by plume in front of the glacier. In fact, upwelling of deep water in front of glacier has been reported for Bowdoin Fjord (Kanna et al., 2018). Since the sediment tolerance of *Calanus* spp. is low (Arendt et al., 2011), it may be hard for them to live in the inner fjord. Due to the large body size and high nutrition, the carcasses of *Calanus* spp. and chaetognaths would be a good food

sources for fishes (Arctic cod) and surface feeding sea birds (Black-legged Kittiwake *Rissa tridactyla*, Glaucous Gull *Larus hyperboreus* and Northern Fulmar *Fulmarus glacialis*), which form massive aggregations at the calving front of the Bowdoin Fjord (Nishizawa et al., submitted).

5. Conclusions

Based on zooplankton samples collected at the surface of Bowdoin Fjord in north-western Greenland, the zooplankton community structure was evaluated using three methods: a microscope, OPC and ZooScan. Among these methods, the analysis by ZooScan was able to filter out abiotic particles. Because of this advantage, it was shown that ZooScan provides more accurate abundance, biomass, size composition and NBSS data than the previously applied microscopic analysis, direct wet mass measurements and OPC measurements. Through analyses, the zooplankton community was clustered into three groups that characterized differences in dominant taxa. The horizontal distribution of the three groups clearly separated each other. The outer groups were dominated by jellyfishes, the middle fjord group was dominated by cypris larvae of barnacles, and the inner groups was characterized by large-sized *Calanus* spp. and chaetognaths. The large-sized zooplankton of the inner group suggests that they were transported from the outer fjord through layers of bottom water, then upwelled by the plume near the calving glacier. Since the large zooplankton contain more nutrition than the zooplankton of the other two groups, the inner fjord near the calving front would be a good feeding ground for fish and sea-birds.

Acknowledgements

We thank Toku Oshima and Drs. Yasushi Fukamachi, Yoshihiko Ohashi, Daiki Sakakibara and Izumi Asaji, who assisted with our field observations. This study was financially supported by the Arctic Challenge for Sustainability (ArCS) project led by Drs. Kumiko Azuma and Toru Hirawake. Part of this study was supported by a Grant-in-Aid for Scientific Research 18K14506 (Early Career Scientists), 17H01483 (A), 16H02947 (B) and 15KK0268 (Joint International Research) from the Japan Society for the Promotion of Science (JSPS).

460 **References**

461 Aksnes, D.L., Aure, J., Kaartvedt, S., Magnesen, T., Richard, J. 1989. Significance of
462 advection for the carrying capacities of fjord populations. Mar. Ecol. Prog. Ser.
463 50, 263−274.

464 Arendt, K.E., Nielsen, T.G., Rysgaard, S., Tönnesson, K. 2010. Differences in plankton
465 community structure along the Godthåbsfjord, from the Greenland Ice Sheet to
466 offshore waters. Mar. Ecol. Prog. Ser. 401, 49−62.

467 Arendt, K.E., Dutz, J., Jónasdóttir, S.H., Jung-Madsen, S., Mortensen, J., Møller, E.F.,
468 Nielsen, T.G. 2011. Effects of suspended sediments on copepods feeding in a
469 glacial influenced sub-Arctic fjord. J. Plankton Res. 33, 1526–1537.

470 Arimitsu, M.L., Piatt, J.F., Mueter, F. 2016 Influence of glacier runoff on ecosystem
471 structure in Gulf of Alaska fjords. Mar. Ecol. Prog. Ser. 560, 19−40.

472 Calbet, A., Riisgaard, K., Saiz, E., Zamora, S., Stedmon, C., Nielsen, T.G. 2011.
473 Phytoplankton growth and microzooplankton grazing along a sub-Arctic fjord
474 (Godthåbsfjord, west Greenland). Mar. Ecol. Prog. Ser. 442, 11−22.

475 Chu, V.W. 2014. Greenland ice sheet hydrology: A review. Prog. Phys. Geogr. 38, 19−54.

476 Colas, F., Tardivel, M., Perchoc, J., Lunven, M., Forest, B., Guyader, G., Danielou, M.M.,
477 Mestre, S.L., Bourriau, P., Antajan, E., Sourisseau, M., Huret, M., Petitgas, P.,
478 Romagnan, J.B. 2018. The ZooCAM, a new in-flow imaging system for fast
479 onboard counting, sizing and classification of fish eggs and metazooplankton.
480 Prog. Oceanogr. 166, 54-65.

481 Dalpadado, P., Hop, H., Rønning, J., Pavlov, V., Sperfeld, E., Buchholz, F., Rey, A., Wold,
482 A. 2016. Distribution and abundance of euphausiids and pelagic amphipods in
483 Kongsfjorden, Isfjorden and Rijpfjorden (Svalbard) and changes in their relative

484 importance as key prey in a warming marine ecosystem. Polar Biol. 39,
485 1765−1784.
486 Field, J.G., Clarke, K.R., Warwick, R.M. 1982. A Practical Strategy for Analysing
487 Multispecies Distribution Patterns. Mar. Ecol. Prog. Ser. 8, 37−52.
488 Gorsky, G., Ohman, M.D., Picheral, M., Gasparini, S., Stemmann, L., Romagnan, J.,
489 Cawood, A., Pesant, S., García-Comas, C., Prejger, F. 2010. Digital zooplankton
490 image analysis using the ZooScan integrated system. J. Plankton Res. 32,
491 285−303.
492 Grosjean, P., Picheral, M., Warembourg, C., Gorsky, G. 2004. Enumeration, measurement,
493 and identification of net zooplankton samples using the ZOOSCAN digital
494 imaging system. ICES J. Mar. Sci. 61, 518−525.
495 Herman, A.W. 1988. Simultaneous measurement of zooplankton and light attenuance
496 with a new optical plankton counter. Cont. Shelf Res. 8, 205−221.
497 Herman, A.W. 1992. Design and calibration of a new optical plankton counter capable of
498 sizing small zooplankton. Deep-Sea Res. 39A, 395−415.
499 Herman, A.W., Harvey, M. 2006. Application of normalized biomass size spectra to laser
500 optical plankton counter net intercomparisons of zooplankton distributions. J.
501 Geophys. Res. 111, C05S05, doi: 10.1029/2005JC002948.
502 Herz, L.E. 1933. The morphology of the later stages of *Balanus crenatus* Bruguiere. Biol.
503 Bull. 64, 432−442.
504 Hop, H., Pearson, T., Hegseth, E.N., Kovacs, K.M., Wiencke, C., Kwasniewski, S., Eiane,
505 K., Mehlum, F., Gulliksen, B., Wlodarska-Kowalczuk, M., Lydersen, C.,
506 Weslawski, J.M., Cochrane, S., Gabrielsen, G.W., Leakey, R.J.G., Lønne, O.J.,
507 Zajaczkowski, M., Falk-Petersen, S., Kendall, M., Wängberg, S., Bischof, K.,

508 Voronkov, A.Y., Kovaltchouk, N.A., Wiktor, J., Poltermann, M., di Prisco, G.,
509 Papucci, C., Gerland, S. 2002. The marine ecosystem of Kongsfjorden, Svalbard.
510 Polar Res. 21, 167−208.
511 Howat, I.M., Eddy, A. 2011. Multi-decadal retreat of Greenland's marine-terminating
512 glaciers. J. Glaciol. 57, 389-396.
513 Kanna, N., Sugiyama, S., Ohashi, Y., Sakakibara, D., Fukamachi, Y., Nomura, D. 2018.
514 Upwelling of macronutrients and dissolved inorganic carbon by a subglacial
515 freshwater driven plume in Bowdoin Fjord, northwestern Greenland. J. Geophys.
516 Res. Biogeosci. 123, 1666-1682.
517 Lydersen, C., Assmy, P., Falk-Petersen, S., Kohler, J., Kovacs, K.M., Reigstad, M., Steen,
518 H., Strøm, H., Sundfjord, A., Varpe, Ø., Walczowski, W., Weslawski, J.M.,
519 Zajaczkowski, M. 2014. The importance of tidewater glaciers for marine
520 mammals and seabirds in Svalbard, Norway. J. Mar. Syst. 129, 452−471.
521 Marcolin, C.R., Schultes, S., Jackson, G.A., Lopes, R.M. 2013. Plankton and seston size
522 spectra estimated by the LOPC and ZooScan in the Abrolhos Bank ecosystem
523 (SE Atlantic). Cont. Shelf Res. 70, 74−87.
524 Marcolin, C.R., Gaeta, S., Lopes, R.M. 2015. Seasonal and interannual variability of
525 zooplankton vertical distribution and biomass size spectra off Ubatuba, Brazil. J.
526 Plankton Res. 37, 808−819.
527 Matsuno, K., Yamaguchi, A., Imai, I. 2012. Biomass size spectra of mesozooplankton in
528 the Chukchi Sea during the summers of 1991/1992 and 2007/2008: an analysis
529 using optical plankton counter data. ICES J. Mar. Sci. 69, 1205−1217.
530 Moore, S.K., Suthers, I.M., 2006. Evaluation and correction of subresolved particles by
531 the optical plankton counter in three Australian estuaries with pristine to highly

532 modified catchments. J. Geophys. Res. 111, C05S04.
533 Motoda, S. 1959. Devices of simple plankton apparatus. Mem. Fac. Fish. Hokkaido Univ.
534 7, 73−94.
535 Murray, T., Scharrer, K., Selmes, N., Booth, A.D., James, T.D., Bevan, S.L., Bradley, J.,
536 Cook, S., Cordero Llana, L., Drocourt, Y., Dyke, L., Goldsack, A., Hughes, A.L.,
537 Luckman, A.J., McGovern, J. 2015. Extensive Retreat of Greenland Tidewater
538 Glaciers, 2000–2010. Arct. Antarct. Alp. Res. 47, 427-447.
539 Nishizawa, B., Kanna, N., Ohashi, Y., Sakakibara, D., Asaji, I., Abe, Y., Yamaguchi, A.,
540 Sugiyama, S., Watanuki, Y. Contrasting communities of seabirds in subglacial
541 meltwater plume and oceanic water in Bowdoin fjord in northwestern Greenland.
542 ICES J. Mar. Sci., submitted.
543 Nogueira, E., González - Nuevo, G., Bode, A., Varela, M., Morán, X.A.G., Valdés, L.
544 2004. Comparison of biomass and size spectra derived from optical plankton
545 counter data and net samples: application to the assessment of mesoplankton
546 distribution along the Northwest and North Iberian Shelf. ICES J. Mar. Sci. 61,
547 508−517.
548 Ohashi, Y., Iida, T., Sugiyama, S., Aoki, S. 2016. Spatial and temporal variations in high
549 turbidity surface water off the Thule region, northwestern Greenland. Polar Sci.
550 10, 270-277.
551 Palma, S., Retamal, M.C., Silva, N., Silva, C. 2014. Horizontal and vertical distributions
552 of siphonophores in relation to oceanographic conditions in Chilean Patagonian
553 fjords. Sci. Mar. 78, 339−351.
554 Riisgaard, K., Swalethorp, R., Kjellerup, S., Juul-Pedersen, T., Nielsen, T.G. 2014.
555 Trophic role and top-down control of a subarctic protozooplankton community.

556 Mar. Ecol. Prog. Ser. 500, 67−82.
557 Sakakibara, D., Sugiyama, S. 2018. Ice front and flow speed variations of marine-
558 terminating outlet glaciers along the coast of Prudhoe Land, northwestern
559 Greenland. J. Glaciol. 64, 300-310.
560 Schultes, S., Lopes, R.M. 2009. Laser Optical Plankton Counter and ZooScan
561 intercomparison in tropical and subtropical marine ecosystems. Limnol.
562 Oceanogr. Methods 7, 771–784.
563 Sprules, W.G., Munawar, M. 1986. Plankton size spectra in relation to ecosystem
564 productivity, size, and perturbation. Can. J. Fish. Aquat. Sci. 43, 1789−1794.
565 Sprules, W.G., Jin, E.H., Herman, A.W., Stockwell, J.D. 1998. Calibration of an optical
566 plankton counter for use in fresh water. Limnol. Oceanogr. 43, 726−733.
567 Sugiyama, S., Sakakibara, D., Tsutaki, S., Maruyama, M., Sawagaki, T. 2015. Glacier
568 dynamics near the calving front of Bowdoin Glacier, northwestern Greenland. J.
569 Glaciol. 61, 223-232.
570 Swalethorp, R., Malanski, E., Agersted, M.D., Nielsen, T.G., Munk, P. 2015. Structuring
571 of zooplankton and fish larvae assemblages in a freshwater-influenced
572 Greenlandic fjord: influence from hydrography and prey availability. J. Plankton
573 Res. 37, 102−119.
574 Thompson, G.A., Dinofrio, E.O., Alender, V.A. 2013. Structure, abundance and biomass
575 size spectra of copepods and other zooplankton communities in upper waters of
576 the Southwestern Atlantic Ocean during summer. J. Plankton Res. 35, 610−629.
577 Vandromme, P., Stemmann, L., Garcìa-Comas, C., Berline, L., Sun, X., Gorsky, G. 2012.
578 Assessing biases in computing size spectra of automatically classified
579 zooplankton from imaging systems: A case study with the ZooScan integrated

system. Methods Oceanogr. 1−2, 3−21.

Vandromme, P., Nogueira, E., Huret, M., Lopez-Urrutia, Á., González-Nuevo González, G., Sourisseau, M., Petitgas, P. 2014. Springtime zooplankton size structure over the continental shelf of the Bay of Biscay. Ocean Sci. 10, 821−835.

Yokoi, Y., Yamaguchi, A., Ikeda, T. 2008. Regional and interannual changes in the abundance, biomass and size structure of mesozooplankton in the western North Pacific in early summer analyzed using an optical plankton counter. Bull. Plankton Soc. Japan 55, 9−24 (in Japanese with English abstract).

Zhang, X., Roman, M., Sanford, A., Adolf, H., Lascara, C., Burgett, R. 2000. Can an optical plankton counter produce reasonable estimates of zooplankton abundance and biovolume in water with high detritus? J. Plankton Res. 22, 137−150.

Zhou, M. 2006. What determines the slope of a plankton biomass spectrum? J. Plankton Res. 28, 437−448.

Zhou, M., Tande, K.S., Zhu, Y., Basedow, S. 2009. Productivity, trophic levels and size spectra of zooplankton in northern Norwegian shelf regions. Deep-Sea Res. II 56, 1934−1944.

Figure/table captions

Fig. 1. Sampling location (a) and latitudinal changes in hydrography (temperature and salinity) (b) in Bowdoin Fjord during 27-29 July 2016. Open symbols: plankton sampling, dotted symbols: CTD measurement.

Fig. 2. Linear regressions of abundance (a) and biomass (b) of the total zooplankton community between different quantitative methods: microscopic count, direct wet mass (WM) measurement, OPC and ZooScan measurements. Each regression indicates the linear fit between one method (*Y*-axis) versus another method (*X*-axis). Factor means *Y*:*X*.

Fig. 3. Results of a cluster analysis based on zooplankton biomass derived from wet mass measurement (a). Three groups (A-C) and two out groups (Out) were identified at 47.5% similarity. The horizontal distribution of each group identified from cluster analysis on zooplankton biomass in the Bowdoin Fjord during 27– 29 July 2016 (b).

Fig. 4. Comparison of abundance, biomass and taxonomic composition, which was quantified by microscopic count and direct measurements (left), and those by ZooScan measurements (right). Labels (Group A-C) below station numbers indicate clustered groups (cf. Fig. 3a).

Fig. 5. Relationships between ZooScan (*Y*-axis) and direct quantification (*X*-axis) on the abundance and biomass of each zooplankton species/taxon. Solid and dashed lines indicate 1:1 and significant relationships between the values, respectively.

Fig. 6. Comparison of abundance, biomass and size composition, which were quantified by OPC (left) and ZooScan (right). Sizes were arranged with five ESD size classes between 0.335-5 mm (0.335-1, 1-2, 2-3, 3-4, 4-5 mm). Labels (Group

620 A-C) below station numbers indicate clustered groups (cf. Fig. 3a).

621 Fig. 7. Relationships between abundance (left) and biomass (right) derived from ZooScan
622 (*Y*-axis) and OPC (*X*-axis) of each zooplankton ESD size class (0.335-1, 1-2, 2-
623 3, 3-4 and 4-5 mm). Solid and dashed lines indicate 1:1 and significant
624 relationship between the values, respectively.

625 Fig. 8. NBSS for zooplankton at each station in the Bowdoin Fjord during 27-29 July
626 2016. Open and solid symbols are the plots derived from OPC and ZooScan,
627 respectively. Dashed and solid lines are the fitted plots of NBSS for OPC and
628 ZooScan, respectively.

629 Table 1. List of NBSS slope and intercept derived from OPC and ZooScan at each station
630 in the Bowdoin Fjord during 27-29 July in 2016.

631 Table 2. Results of ANCOVA for the slope of NBSS, with the intercept of NBSS and
632 differences in instrument (i.e., OPC or ZooScan) applied as independent
633 variables.

634

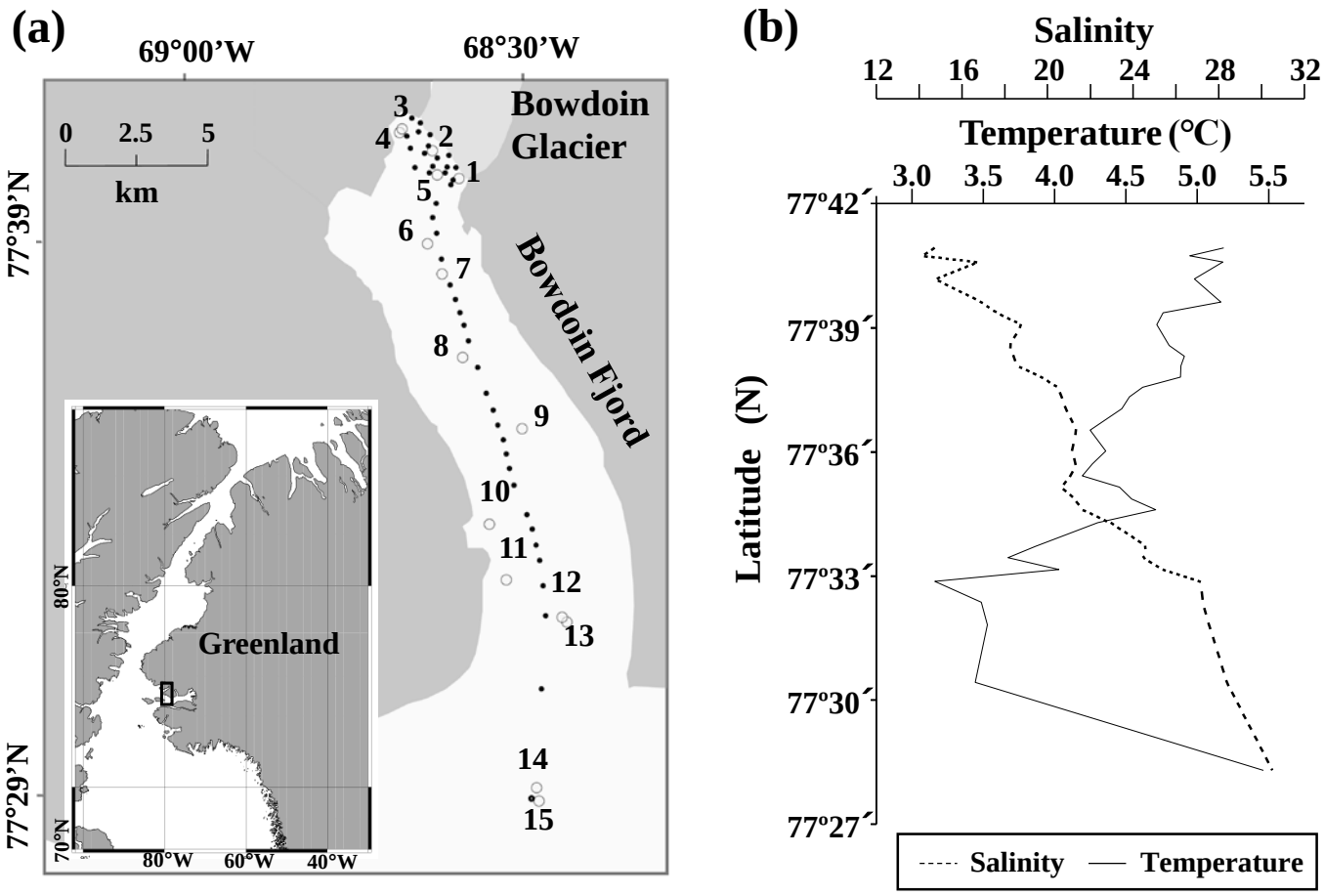

Fig. 1. Sampling location (a) and latitudinal changes in hydrography (temperature and salinity) (b) in Bowdoin Fjord during 27-29 July 2016. Open symbols: plankton sampling, dotted symbols: CTD measurement.

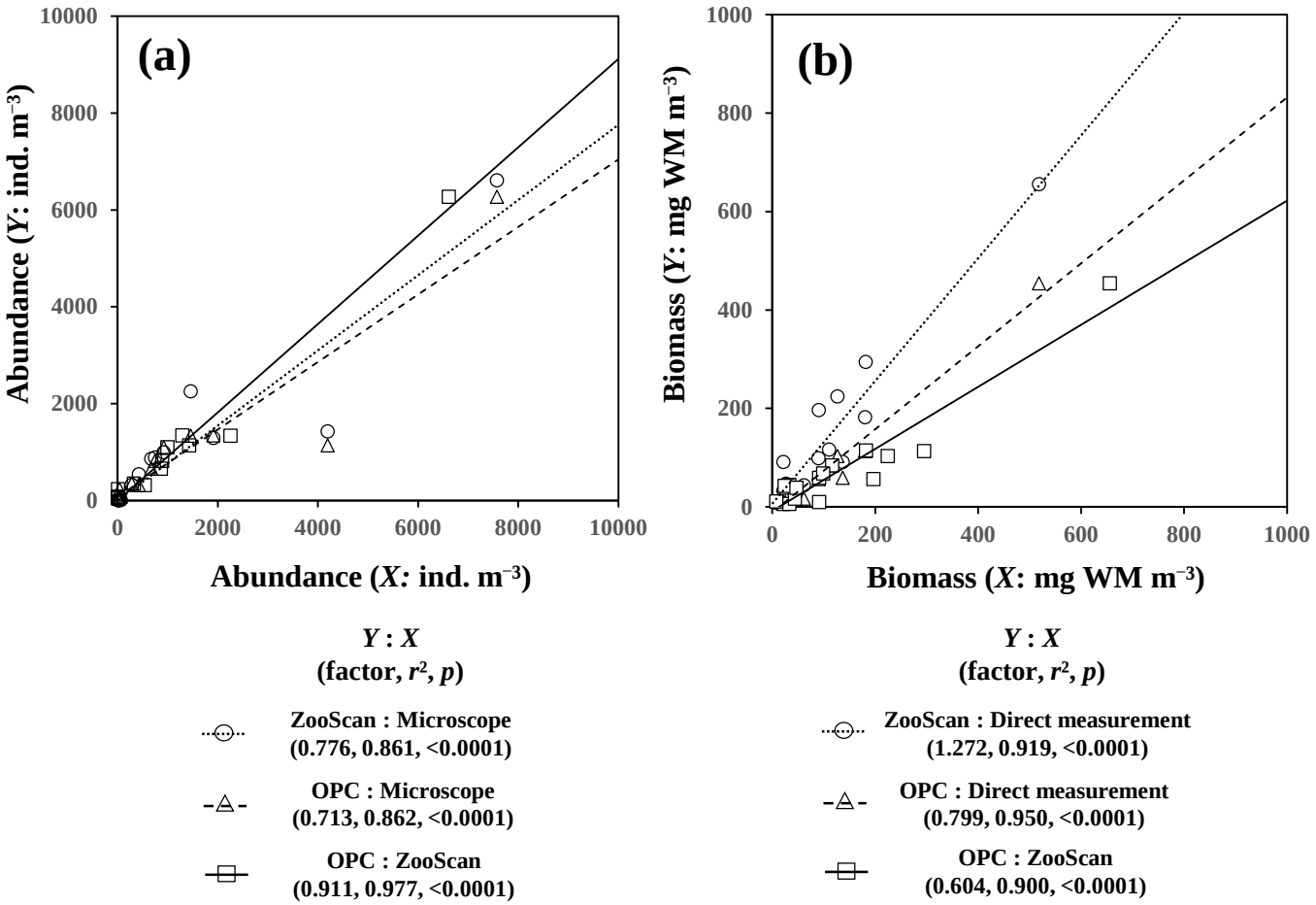

Fig. 2. Linear regressions of abundance (a) and biomass (b) of the total zooplankton community between different quantitative methods: microscopic count, direct wet mass (WM) measurement, OPC and ZooScan measurements. Each regression indicates the linear fit between one method (*Y*-axis) versus another method (*X*-axis). Factor means *Y*:*X*.

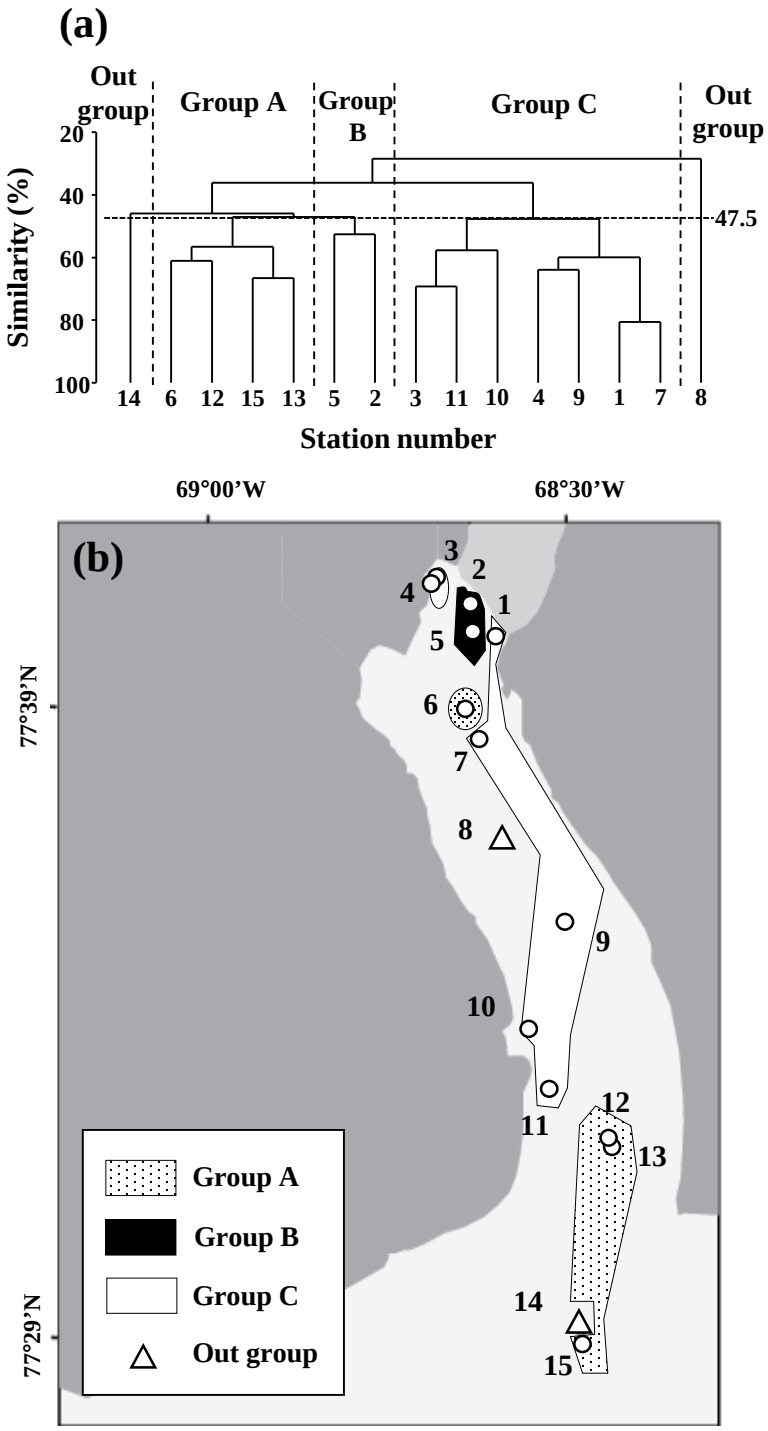

Fig. 3. Results of a cluster analysis based on zooplankton biomass derived from wet mass measurement (a). Three groups (A-C) and two out groups (Out) were identified at 47.5% similarity. The horizontal distribution of each group identified from cluster analysis on zooplankton biomass in the Bowdoin Fjord during 27– 29 July 2016 (b).

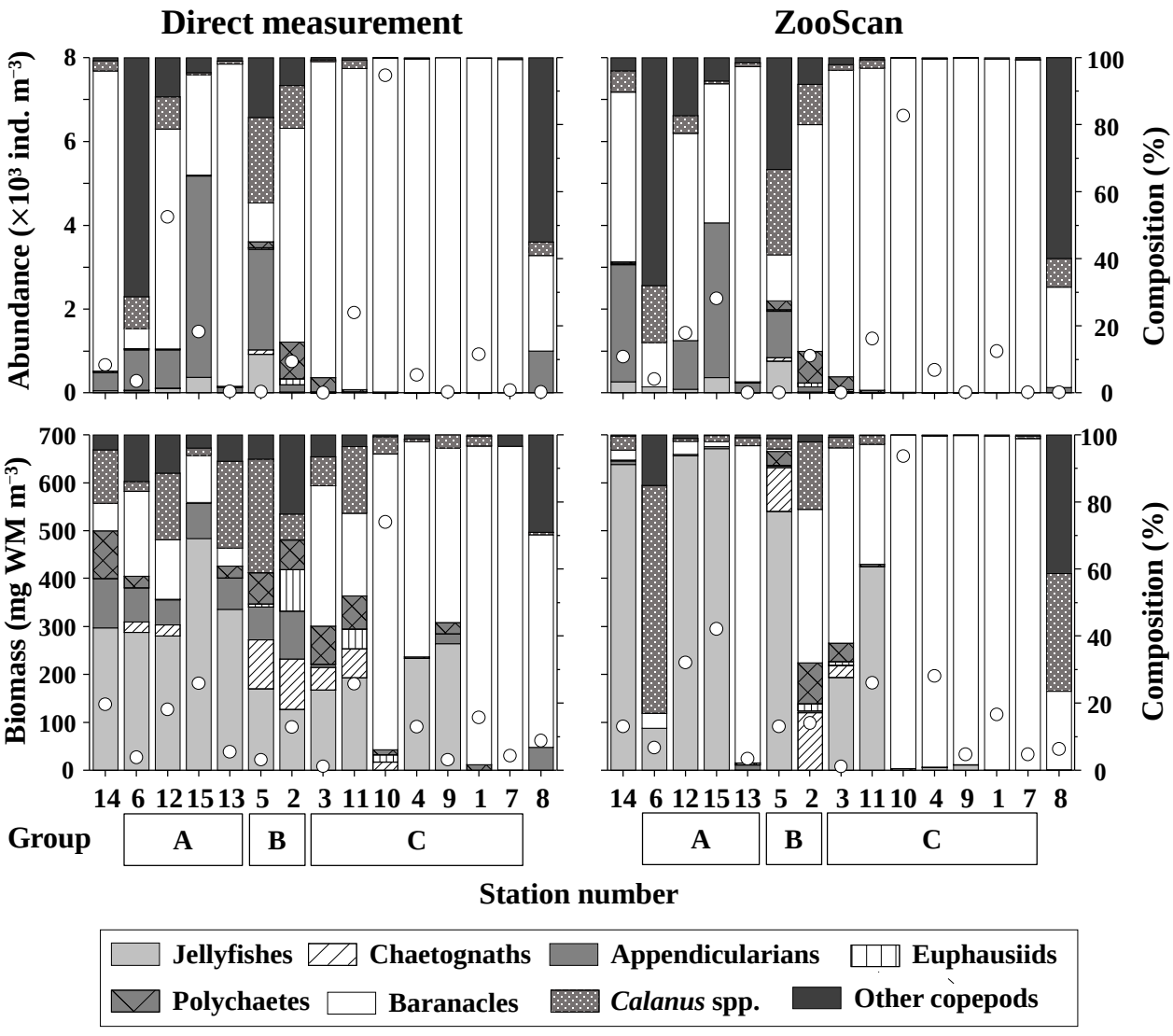

Fig. 4. Comparison of abundance, biomass and taxonomic composition, which was quantified by microscopic count and direct measurements (left), and those by ZooScan measurements (right). Labels (Group A-C) below station numbers indicate clustered groups (cf. Fig. 3a).

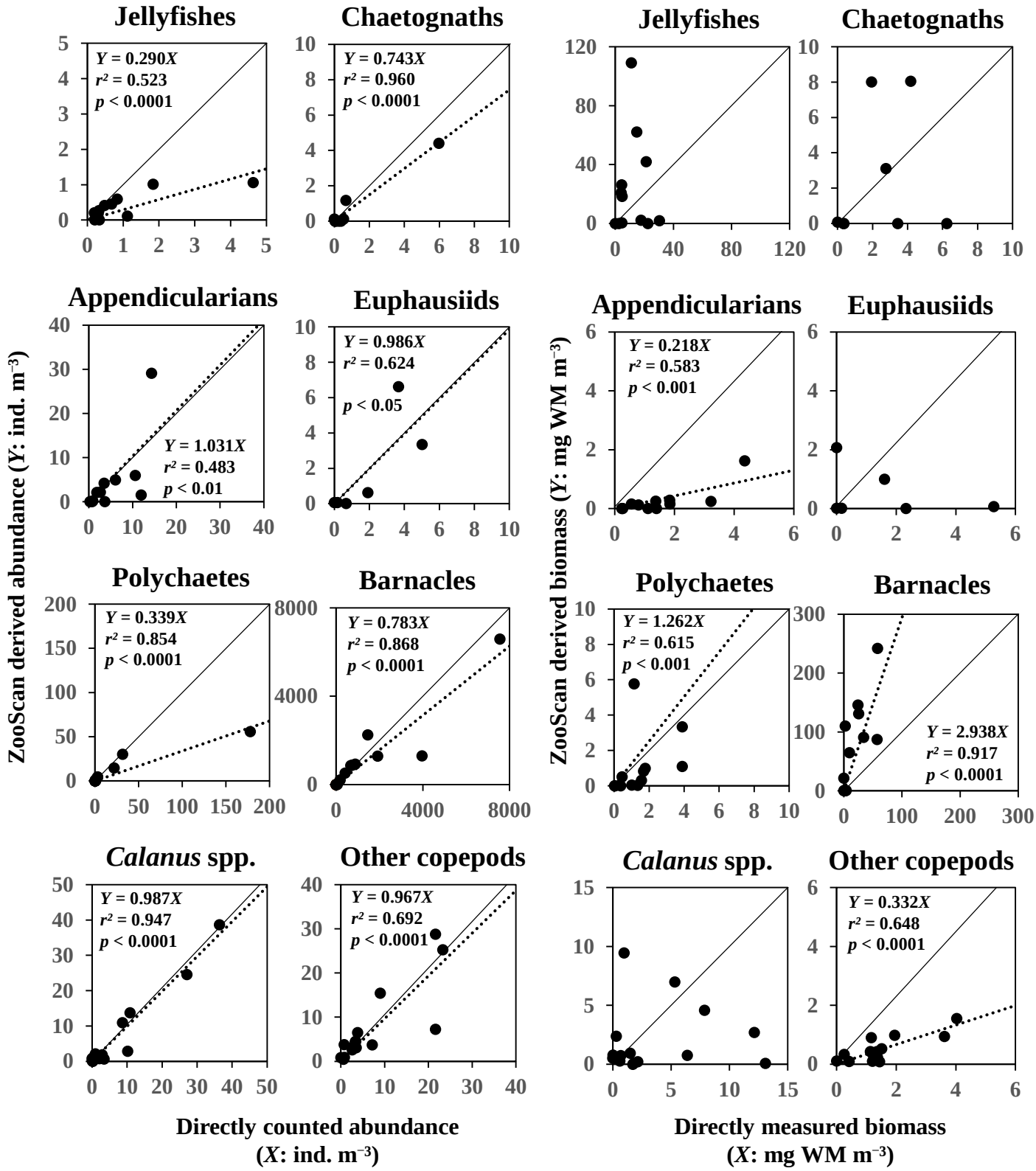

Fig. 5. Relationships between ZooScan (*Y*-axis) and direct quantification (*X*-axis) on the abundance and biomass of each zooplankton species/taxon. Solid and dashed lines indicate 1:1 and significant relationships between the values, respectively.

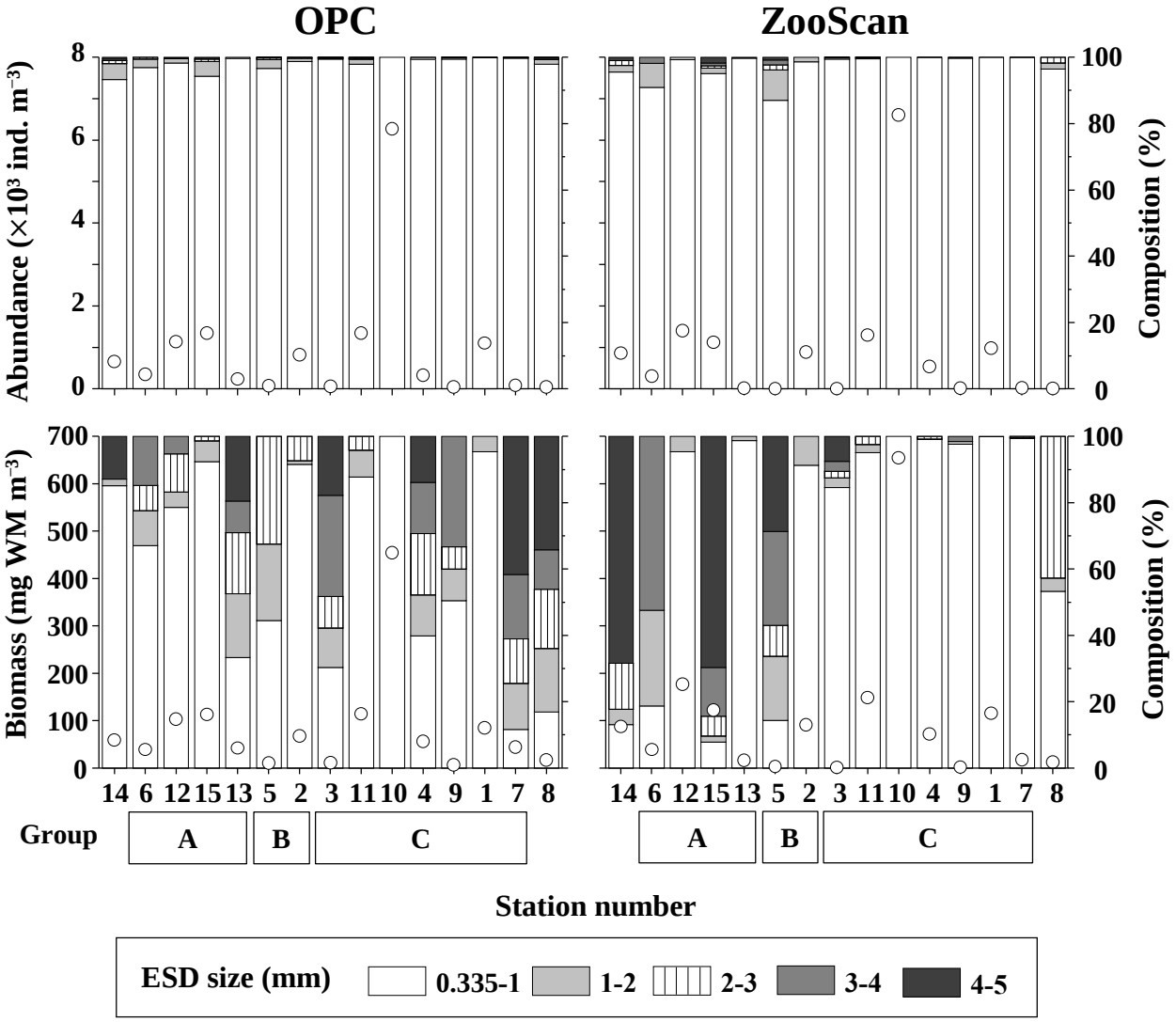

Fig. 6. Comparison of abundance, biomass and size composition, which were quantified by OPC (left) and ZooScan (right). Sizes were arranged with five ESD size classes between 0.335-5 mm (0.335-1, 1-2, 2-3, 3-4, 4-5 mm). Labels (Group A-C) below station numbers indicate clustered groups (cf. Fig. 3a).

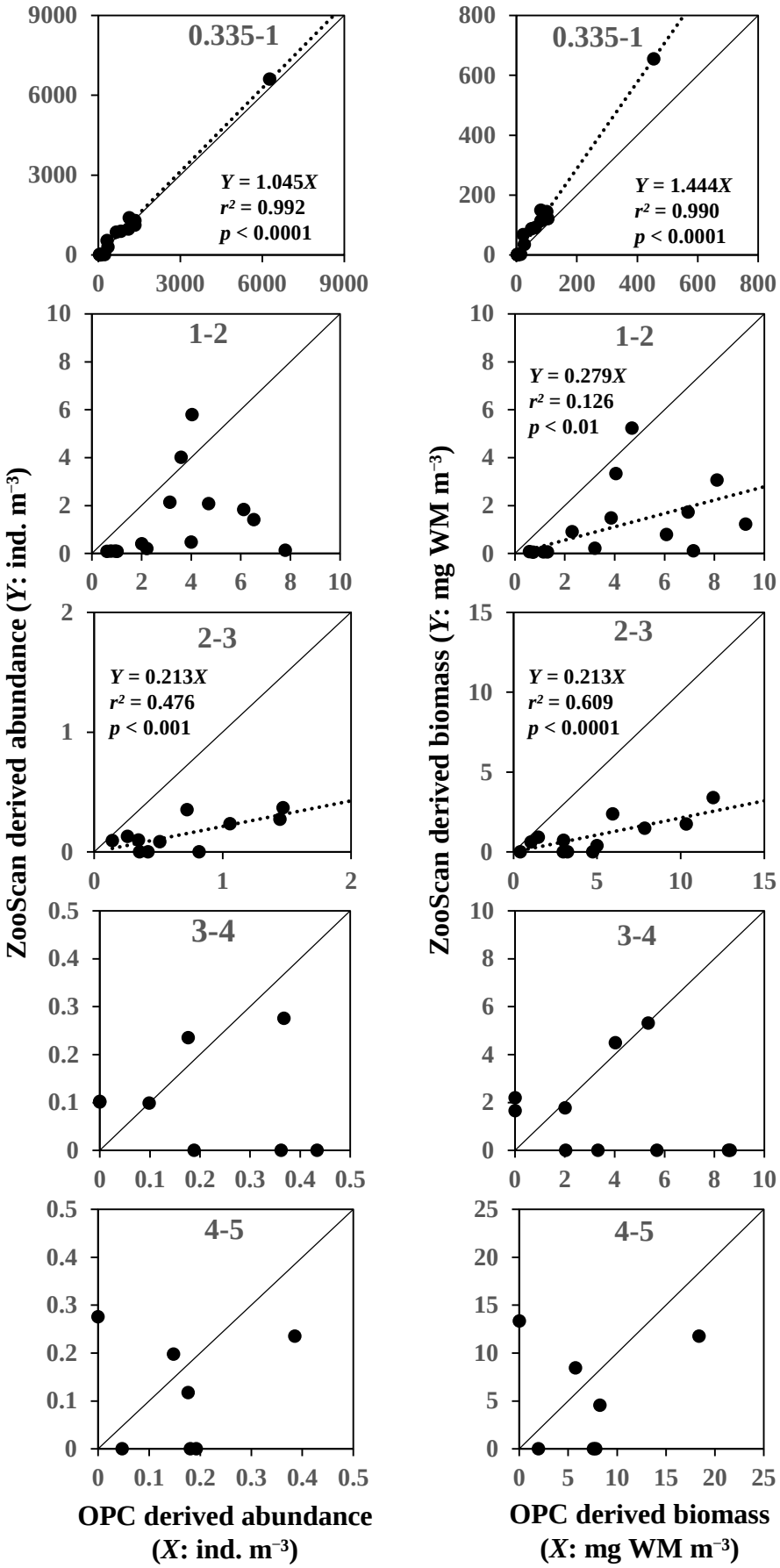

Fig. 7. Relationships between abundance (left) and biomass (right) derived from ZooScan (*Y*-axis) and OPC (*X*-axis) of each zooplankton ESD size class (0.335-1, 1-2, 2-3, 3-4 and 4-5 mm). Solid and dashed lines indicate 1:1 and significant relationship between the values, respectively.

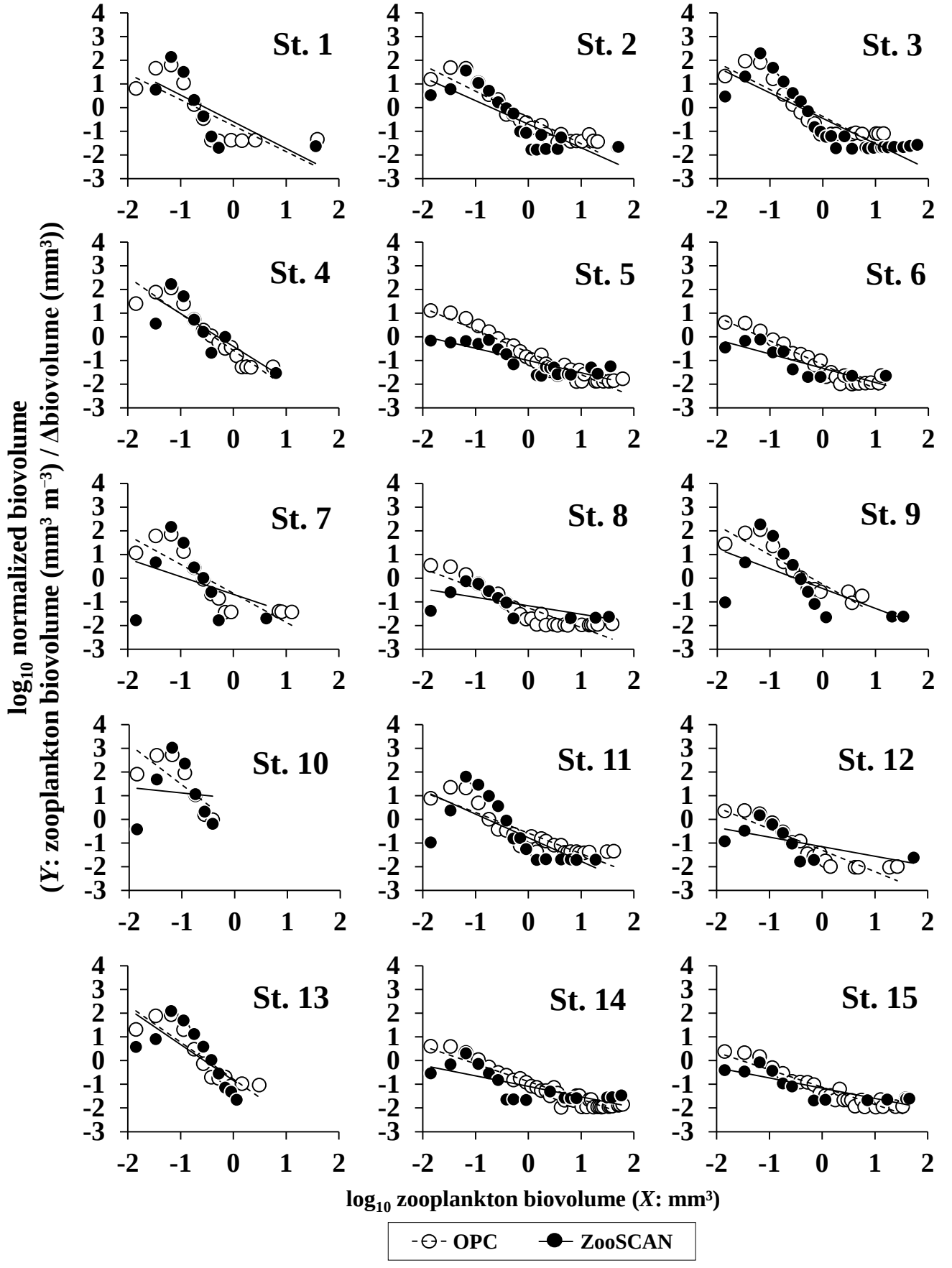

Fig. 8. NBSS for zooplankton at each station in the Bowdoin Fjord during 27-29 July 2016. Open and solid symbols are the plots derived from OPC and ZooScan, respectively. Dashed and solid lines are the fitted plots of NBSS for OPC and ZooScan, respectively.

Table 1. List of NBSS slope and intercept derived from OPC and ZooScan at each station in the Bowdoin Fjord during 27-29 July in 2016.

	NBSS derived from OPC			NBSS derived from ZooScan		
Station	Slope	Intercept	r^2	Slope	Intercept	r^2
1	-1.096	-0.762	0.608	-1.130	-0.597	0.520
2	-1.110	-0.415	0.877	-0.995	-0.697	0.686
3	-1.136	-0.368	0.806	-1.077	-0.451	0.739
4	-1.551	-0.578	0.882	-1.390	-0.407	0.650
5	-0.942	-0.656	0.931	-0.516	-1.005	0.732
6	-1.012	-1.179	0.915	-0.602	-1.326	0.720
7	-1.222	-0.639	0.751	-0.744	-0.685	0.137
8	-0.828	-1.258	0.832	-0.358	-1.168	0.427
9	-1.242	-0.262	0.835	-0.839	-0.443	0.385
10	-1.705	-0.245	0.607	-0.229	0.889	0.008
11	-0.868	-0.581	0.809	-0.997	-0.774	0.515
12	-0.905	-1.306	0.850	-0.406	-1.154	0.361
13	-1.562	-0.784	0.816	-1.516	-0.836	0.561
14	-0.747	-0.884	0.908	-0.446	-1.088	0.565
15	-0.737	-1.121	0.866	-0.433	-1.164	0.715

Table 2. Results of ANCOVA for the slope of NBSS, with the intercept of NBSS and differences in instrument (i.e., OPC or ZooScan) applied as independent variables.

Parameter	d.f.	SS	*F*-value	*p*-value
Intercept	1	0.304	2.423	0.1316
Instrument	1	0.304	6.538	0.0167
Instrument×Intercept	1	0.311	2.477	0.1276